Manufacturing of perovskite oxygen carriers by spray granulation for chemical looping combustion

Vincent Thoréton †, Ove Darell†††, Aud I Spjelkavik††, Martin Fleissner Sunding††, Tommy Mokkelbost†††, Mehdi Pishahang††, Kjell Wiik†, Yngve Larring††*

† Department of Materials Science and Engineering, Norwegian University of Science and Technology, Trondheim, Norway.

†† SINTEF Materials and Chemistry, P.O. Box 124 Blindern, NO-0314 Oslo Norway.

††† SINTEF Materials and Chemistry, NO-7465 Trondheim, Norway.

* To whom correspondence should be addressed.

Corresponding Author

Dr. Yngve Larring - Phone: (+47)-982-83-956

E-mail: Yngve.Larring@sintef.no.

Keywords: CLC, oxygen carrier material, calcium manganite, CMTF, CMT

ABSTRACT:

Chemical looping combustion is a technology under development allowing power production with inherent separation of CO_2 during fuel combustion. Its principle relies on oxygen carrier materials which transport oxygen from the air to oxidise the fuel. One challenge is to develop and produce materials with suitable chemical and physical properties, low environmental impact, while minimising the cost of production. Here we demonstrate that spray granulation, a scalable industrial process, is relevant to manufacture promising oxygen carrier materials from low cost and low environmental impact minerals and with good mechanical properties: $Ca_{0.98}Mn_{0.875}Ti_{0.125}O_3$ and $Ca_{0.98}Mn_{0.75}Fe_{0.125}Ti_{0.125}O_3$. Iron substitution clearly reduces the sintering time. Increasing the calcination temperature and calcination time enhances the bulk density and resistance against physical attrition.

1. Introduction

Global energy production, inherited from the second industrial revolution, is based on more than 80% of non-renewable fossil energies, i.e. oil, coal and gas. Nevertheless, fossil resources are finite. Their availability decreases, followed by an increase of the production cost. Overall, the massive use of fossil resources over the last century contributes to an accelerated climate change [1]. Using fossil resources for energy production is economically and environmentally not sustainable in the end. An energetic transition, including a better distribution and an overall decrease in the consumption, is necessary. Carbon capture storage and usage (CCS and CCU) can play an important role during the transition period. Carbon dioxide (CO_2) capture from existing power plants and industries is already achievable by different and complementary technologies such as amine scrubbing or calcium looping. The start in the development of CO_2

capture technologies goes back to over four decades ago, however the CO_2 capture technologies have been more coupled with enhanced oil recovery (EOR) during the past ten years [2]. As for storage of CO_2, it offers the possibility to limit the emissions of this greenhouse gas in the atmosphere. By using biomass as a fuel, bio-CCS offers even the possibility of negative emission of CO_2. As an efficient power generation technology with close to complete capture capability, Chemical Looping Combustion (CLC) provides a promising technological possibility for transition towards renewable energies. Both amine scrubbing and calcium looping have capture efficiency close to 90%. However some amines' toxicity presents a threat for human health and the environment [3]. Public acceptance is necessary for further development of CCS. The development of the next generation of transitory power plants should aim at safer operation and higher capture efficiency. CLC shows a great potential, high efficiency combined with one of the lowest cost for CO_2 capture [4-5]. Unlike other capture techniques, CLC allows power production with inherent separation of CO_2 during the fuel combustion. The fuel combustion is performed with oxygen provided by a solid oxygen carrier material (OCM), preventing the fuel to be mixed with nitrogen. After condensation of water at the exhaust, the process provides a pure CO_2 stream. The concept and latest achievements have been described elsewhere [6-9].

Several configurations are possible for CLC. The most common approach is based on the interconnection of two circulating fluidised beds (CFB) reactors. One is fed with air, the other with fuel; the OCM flows continuously through the two reactors. An alternative CLC configuration is a set of alternating reactors, which could be either fixed bed or bubbling bed reactors. In this case, the OCM is kept inside a reactor and exposed to alternating gas feeds [10-12]. It is also considered to adapt the CLC principle for other purposes involving partial combustion and production of syngas [13]. The targeted properties of OCM are dependent on the

63 configuration and application. In the case of CFB-CLC, the OCM must retain good mechanical
64 properties, i.e. low fragmentation, attrition and agglomeration along redox cycles as well as high
65 reactivity (improved by high porosity). These properties should be combined with a low cost.
66 These requirements are commonly counteracting and a compromise must be found.

67 First, the composition of the OCM matters. Several hundreds of materials based on Ni, Cu, Fe,
68 Mn and Co, and combination of these, have been studied as potential OCM [6, 14-16]. Nickel oxide
69 supported on alumina ($Ni/NiAl_2O_4$) was extensively studied and is established as a reference
70 material. However, this material is both expensive and toxic. On the other hand, the use of low
71 cost environmentally-friendly minerals like ilmenite[17], manganese[18] or iron [19-20] ores have
72 also been considered. This approach is suitable to decrease the cost, especially for combustion of
73 solid fuel, in which case ashes will shorten the OCM lifetime. The overall performance of these
74 minerals is often below the one of synthetic materials. The OCM properties of the minerals may
75 however be enhanced by thermal activation [21] or appropriate addition of other oxides [20].
76 Lately, a significant interest has been shown towards perovskite-type oxides [22], especially those
77 derived from the calcium manganite ($CaMnO_{3-\delta}$) family. Substitution of Mn by magnesium [23],
78 titanium [24-26] or a combination of both [27-28] have been investigated. It has been demonstrated
79 that $CaMn_{0.875}Ti_{0.125}O_{3-\delta}$ (CMT) is a promising OCM [29-31]. Furthermore, it has been shown that
80 iron substitution improves the spontaneous release of oxygen (later called Chemical Looping
81 Oxygen Uncoupling or CLOU) properties, provides higher conversion [32] and less degradation
82 of the microstructure (to be published). The way of manufacturing the OCM is the second
83 decisive factor. OCM may be produced by different techniques such as freeze-drying (laboratory
84 scale) [25], impregnation [33], spray drying [34-35] or simply milling and sieving of raw materials
85 [20]. In the present investigation, it was chosen to produce OCM by spray granulation. This

process allows homogeneous mixing of different components and good control of granule particle size. It is a common process in chemical, pharmaceutical and food industries [36]. Compared to spray drying, spray granulation allows an easier control of the particle size by residence time inside the process chamber. Spray granulation also use a lower temperature compared to spray drying and generally results in more porous particles.

Here, three types of granules were successfully produced by spray granulation or spray coating and subsequent sintering in air from low-cost industrial quality chemicals with low environmental impact. Two types of self-supported OCM, based on the promising calcium manganite titanate perovskite were investigated: CMT ($Ca_{0.98}Mn_{0.875}Ti_{0.125}O_3$) and CMTF125 ($Ca_{0.98}Mn_{0.75}Fe_{0.125}Ti_{0.125}O_3$) with 12.5% of iron on the B-site of the perovskite. The performance characteristics of these two materials as OCM for fluidized bed CLC is separately published [28, 37]. CMTF125 was also coated on α-alumina (CMTF125@Alumina). The composition, macrostructural and microstructural properties of the granules were evaluated as well as their mechanical properties at ambient temperature in air.

2. Results and discussion

2.1 Spray granulation and spray coating

Spray granulation is a fairly controllable and reproducible process, and the granules of self-supported OCM were readily obtained. However, the spray coating process was not fully optimised, as the coating of CMTF125@Alumina produced a mixture of the expected coated granules and a non-negligible amount of self-supported CMTF125 granules. Those two types of granules could not be separated. In spite of this practical issue, we chose to investigate the spray

coated granules, but it should be emphasized that the granules made in this way are a mixture of self-supported OCM and spray coated alumina.

2.2 Heat treatments

Before heat treatment, the green-state granules are porous particles composed of different precursors ($CaCO_3$, Mn_3O_4, TiO_2 and Fe_2O_3) bonded with PVA. Due to the weak bonding in between the solid precursors, their reactivity is low. In comparison with an intimate and compact mixture of the precursors, a higher temperature and a longer sintering time are necessary to complete the reaction. Due to extended sintering and reaction with the alumina crucible above 1300˚C, the sintering temperature of CMT and CMTF125 was limited to 1280˚C. CMT granules were sintered for 6 and 12 hours at 1280˚C. CMTF125 granules were heat-treated from 30 minutes to 12 hours in air from 1200˚C to 1280˚C. At these conditions, granules shrank during heat-treatment with a volume reduction close to 25%. Before coating CMTF125 on alumina, highly reactive γ-Al_2O_3 was converted to α-Al_2O_3 in order to lower the reactivity of alumina toward the precursors coated afterwards. After sintering, a shell of the perovskite phase formed around the α-Al_2O_3 core. However, reaction between the perovskite and α-Al_2O_3 was observed at the interface. Details will be given in the following sections.

2.3 Phase analysis

After sintering, we observed that the granules are composed of a perovskite as the main phase and of a spinel as a secondary phase. This was expected from the calcium deficit which was introduced and the fact that there is likely no solid solution in the $Ca(Mn,Ti)_2O_4$ / $Ca(Mn,Ti)O_3$ system as reported for $Ca_{1-y}MnO_3$ [38]. It is worth noting that the calcium deficit was introduced in order to lower the activity of Ca and to limit the reaction with SO_x and CO_2 as well as to

reduce the formation of Ruddlesden-Popper phases [38], which might reduce the redox kinetics. X-Ray diffractograms of selected samples, sintered for different amounts of time are shown in Figure 1. Those were normalized with respect to the main peak of the perovskite phase. During the heat treatment, the perovskite was formed, along with a spinel phase and an intermediate Ruddlesden-Popper phase. The Ruddlesden-Popper phase was generally not detectable in the conditions of the acquisition. The peaks of the spinel are indicated, showing that the formation of the perovskite phase is supported by the iron substitution. Indeed, after 12 hours, the reaction was not fully completed for the CMT compound (Figure 1-a). The same progress was obtain in a shorter time, close to one hour for CMTF125 (Figure 1-b). CMTF125@Alumina showed the same composition behaviour as CMTF125 (Figure 1-c).

2.4 Macro-structure

SEM micrographs of sintered and sieved granules of CMT and CMTF125 granules are shown in Figure 2, showing that spray granulation allows the formation of rather round granules. Typically, mean roundness of granules increases as a function of the mean particle size as illustrated in Figure 3-a. We observed that the roundness of granules larger than 300 µm is typically close to 0.9. It is expected that a higher sphericity will be beneficial with respect to reduced attrition of the granules. However, after sieving in the 125-250 µm range, the resulting roundness is typically between 0.4 and 1.0 with the median close to 0.75 as illustrated in Figure 3-b. The corresponding particle size distributions are shown in Figure 3-a. The differences observed are inherent to the spray granulation step.

2.5 Microstructure

2.5.1 Green-state granules

SEM micrographs and corresponding EDS maps of the cross-section of a typical green-state granule are shown in Figure 4-a. The precursors are well dispersed. However, the presence of relatively large (50-100 μm) particles of $CaCO_3$ is significant. This is consistent with the particle size analysis shown in Figure 4-b. It seems that the presence of those large particles could affect the reactivity during sintering (see the following paragraphs). Using precursors with smaller particle size is expected to improve the reactivity during the calcination/sintering step but also the granules' sphericity and consequently their mechanical properties.

2.5.2 Self-supported sintered granules (CMT and CMTF125)

The details of the granules' surface, shown in insert in Figure 2, show that the sintering time has a significant influence on the microstructure with a clear effect of sintering duration on the grain growth and densification at the surface. The distribution of the different cations is generally homogeneous. Local inhomogeneity was noticed occasionally, as shown for example in a CMT granule (Figure 5-a). The inhomogeneity is consistent with the observation of large calcium carbonate particles in the green-state granules, as illustrated in a CMTF125 granule sintered at 1200°C (Figure 5-b). The calcium deficient/manganese rich areas are likely to be related to the presence of a spinel phase. However, CMTF125 granules sintered at 1280°C for 12 hours show a high degree of homogeneity and high density (Figure 5-c). The specific surface area of granules as a function of temperature and duration of the sintering step is shown in Figure 6. It is rather low, as expected from the way of synthesis, and clearly decreases with both the sintering temperature and sintering time. Overall, this is in good agreement with the observations of Jing *et al.* on $CaMn_{0.9}Mg_{0.1}O_{3-\delta}$ made by spray drying [39].

2.5.3 Alumina-supported sintered granules (CMTF125@Alumina)

SEM micrographs and corresponding EDS maps of the cross-section of CMTF125@Alumina are shown in Figure 7. The perovskite shell is rather homogeneous. However, it reacts with the alumina core at its interface as iron, titanium and manganese segregate at the surface of the alumina support. It appears that calcium, manganese and iron cations tend to diffuse into the alumina core while aluminium cations diffuse in the opposite direction. An manganese rich layer (together with iron and titanium) is clearly visible inside the alumina particle: it progresses toward the alumina core over time as shown in the cross-sections displayed in Figure 7. Even though the diffusion mechanism is not fully understood, it is expected that the cationic inter-diffusion provides a good adhesion of the CMTF125 shell on the alumina core. However, further diffusion may occur over time as observed after 12 hours at 1280°C. Extensive cationic inter-diffusion of the CMTF125 shell with the alumina core may decrease both the mechanical strength and the reactivity of the granules.

2.6 Mechanical properties and life expectancy

The mechanical strength of the OCM used in CFB-CLC process is an essential property that strongly influences the lifetime of the material. The collisions between the fluidized granules as well as with the reactor walls cause attrition and produce fines corresponding to a gradual break down of the granules. Measuring the mass of an oxygen carrier lost into fines during operation in a chemical looping combustor is a common way to estimate its lifetime [34, 40]. As for accelerated cold attrition test, it allows a fast evaluation of the mechanical attrition behaviour of the material, therefore of its lifetime [41]. On the other hand, one must be cautious in the latter case since it does not measure the attrition due to redox cycling occurring in an operating chemical looping combustor. The lifetime expectancy, limited to the mechanical attrition, was estimated here by comparing the results of the cold attrition test to the one of a $Ni/NiAl_2O_4$ reference made by

196 VITO. Linderholm & *Al.* estimated the lifetime of this material at 33,000 hours [34]. It is delicate
197 to extrapolate the lifetime of our material on this value that has been extrapolated from
198 measurements made in different conditions. However, this simple estimation predicts a lifetime
199 of the same order of magnitude than the most resilient materials. During the mechanical attrition
200 test, only 2% of the reference sample was lost into fines (0.4% per hour). The life-time
201 expectancy of the samples was simply estimated from their weight loss rate, standardised to the
202 one of the reference and is shown in Table 1, as a function of the sintering conditions. The mass
203 loss of selected materials during accelerated cold attrition test is shown in Figure 8. From the
204 attrition behaviour of CMTF125 granules sintered for 30 minutes to 12 hours from 1200 to
205 1280°C, it is clear that the mechanical strength increases with the sintering temperature and
206 sintering duration up to 6 hours while the specific surface area decreases as shown previously in
207 Figure 6. For the longest sintering time (12 hours), the trend reverses, suggesting that the
208 granules get more brittle. This might be due to the increasing grain size, as illustrated in Figure 2
209 (b and c). This seems to indicate that there is an optimum sintering time, probably close to 6
210 hours, at which the granules are dense enough but with small enough grain size to maximise their
211 mechanical strength. On the contrary, a poor homogeneity and a relatively high porosity are
212 expected to be highly detrimental to mechanical strength as observed for example on CMTF125
213 granules sintered at 1200°C. In the latter case, a large shift in the particle size distribution before
214 and after the attrition test is observed in Figure 9. The corresponding shift was limited for the
215 granules sintered at higher temperature and decreased with the duration of the sintering. Both
216 CMTF125@Alumina and CMTF125 have the same life-time expectancy. It seems that coating of
217 CMTF125 on alumina does not affect its mechanical strength. However it seems there is no

obvious advantage of coating CMTF125 on alumina, mainly because the active shell may react with the alumina core overtime.

3. Conclusion

Granules with suitable homogeneity were successfully produced by spray granulation from low-cost industrial quality chemicals. Sintering was investigated, showing that iron substitution reduces the sintering time. The mechanical strength of the granules, their chemical homogeneity and their density increase with a the sintering time, up to an optimum, close to 6 hours at 1280˚C for the CMTF125 self-supported granules. CMTF125 was also successfully coated on α-Al_2O_3 with strong adhesion of the OCM on the substrate. With intrinsically good mechanical properties and good redox properties, CMTF125 is a promising self-supported OCM.

4. Experimental Procedure

4.1 Manufacturing of Oxygen Carrier Materials

All oxygen carrier materials examined in this study were made by spray granulation or spray coating using the following precursors: $CaCO_3$ (Miljøkalk Kalkstein, Fanzefoss Miljøkalk AS), Mn_3O_4 (Micromax, Elkem ASA), TiO_2 (Merck) and Fe_2O_3 (Aldrich). Water-based slurry was made from the above precursors, tap water and PVA (Merck) as a binder. PVA content was 1.6 wt% and the solid/liquid mass ratio equal to 0.90. OCM granules were produced either by spray granulation (self-supported OCM) or by spray coating on α-Al_2O_3 (alumina supported OCM) using a Glatt ProCell Labsystems with a spouted bed insert. The principle of spray granulation and spray coating are illustrated in Figure 10. The slurry was stirred overnight with a blender then warmed up on a heating plate at 60°C. The slurry was continuously stirred during the

process. Air flow, pump speed and nozzle pressure were gradually adjusted to achieve good granulation conditions, aiming at granules in the range of 125 to 250 µm, both for self-supported and alumina supported granules.

Self-supported OCM granules were produced by directly spraying the slurry in the chamber (in-situ generation of seeds) or by spraying on previously grown seeds of the same composition. For alumina-supported OCM, α-Al_2O_3 seeds (diameter: 70-80 µm) were made from γ-Al_2O_3 (Puralox SCCa-5/200) by heat-treatment at 1300°C for two hours in air. The α-Al_2O_3 seeds were coated with the slurry.

The as-made green-state granules were preliminary sieved in the range of 125 to 250 µm. Calcination and sintering were performed in one single step at different temperatures and times under static air, in a large alumina crucible to promote sufficient access to air. Heating and cooling rates were set at 200 and 300°C per hour respectively. The sintered OCM were sieved carefully in the range of 125 to 180 µm after heat treatment. The different samples of granules considered in this study are listed in Table 2.

4.2 Characterisations

X-ray diffraction (XRD) was performed on a Bruker Da Vinci diffractometer with a LinxExe XE detector using CuKα radiation. Data were collected on finely crushed samples from 10° to 60° using a step size of 0.013° and with variable slits. Scanning electron microscopy (SEM) was performed using a Hitachi S-3400N microscope equipped with an EDS Oxford X-Max detector. To evaluate size and shape of the granules, several thousands of particles were widely spread on a transparent sheet to avoid merging and pictured using an Epson V700 high resolution (3200dpi) scanner and analysed using ImageJ [42] software with a home-made macro. Roundness was the most relevant indicator of the granules shape. It is closely related to the actual sphericity,

taking aside the preferential orientation the granules can possibly take [43]. The roundness was calculated as follows for each particle: R= [Minor] / [Major] where “Minor” and “Major” are the dimensions of respective axis of the best fitting ellipse.

The mechanical strength of the granules was evaluated with respect to their attrition behaviour. A home-made accelerated attrition set-up was used following the ASTM E728 standard. A standard protocol during 300 minutes was used for all experiments. For each test, 50 g of material sieved in the range of 125µm to 180µm was used. During the test, the granules broke down, producing fines (< 40 µm) which were collected in a filter. The mass of fines collected in the filter (i.e. the weight loss of initial granules) was measured over time. The size of the granules after attrition was compared to the size prior to testing using an optical light microscope (Leica M420) and the Fiji [44] software for analysis of size and numbers. The particle size was define as the diameter of a circle with an area equivalent to the particle's area. The volume fraction in each size category is based on the average volume of spheres within each size category. Specific surface area was measured by helium adsorption using BET method (Micromeritics Tri Star 3000 Surface Analyzer). A Horiba LA-960 wet particle size analyser was used to measure the particle size distribution of the precursors.

ACKNOWLEDGMENT

This work forms part of the BIGCLC Phase III project supported by the Research Council of Norway (id 224866 and id 193816). The work has additionally been produced with support from the BIGCCS Centre, performed under the Norwegian research program Centres for Environment-friendly Energy Research (FME). The authors acknowledge the following partners

for their contributions: Aker Solutions, Gassco, Shell, Statoil, TOTAL, GDF SUEZ and the Research Council of Norway.

5. REFERENCES

Uncategorized References

[1] *Inventory of U.S. Greenhouse Gas Emissions and Sinks: 1990-2013*, Environemntal Protection Agency, **2015**.

[2] L. S. Melzer, Melzer Consulting, http://neori.org/Melzer_CO2EOR_CCUS_Feb2012.pdf, **2012**.

[3] K. Veltman, B. Singh, E. G. Hertwich, *Environmental Science and Technology* **2010**, *44*, 1496-1502.

[4] A. Lyngfelt, B. Leckner, T. Mattisson, *Chemical Engineering Science* **2001**, *56*, 3101-3113.

[5] M. E. Boot-Handford, J. C. Abanades, E. J. Anthony, M. J. Blunt, S. Brandani, N. Mac Dowell, J. R. Fernández, M.-C. Ferrari, R. Gross, J. P. Hallett, R. S. Haszeldine, P. Heptonstall, A. Lyngfelt, Z. Makuch, E. Mangano, R. T. J. Porter, M. Pourkashanian, G. T. Rochelle, N. Shah, J. G. Yao, P. S. Fennell, *Energy & Environmental Science* **2014**, *7*, 130.

[6] M. M. Hossain, H. I. de Lasa, *Chem. Eng. Sci.* **2008**, *63*, 4433-4451.

[7] H. Fang, L. Haibin, Z. Zengli, *International Journal of Chemical Engineering* **2009**, *2009*, 16.

[8] J. Adanez, A. Abad, F. Garcia-Labiano, P. Gayan, L. F. de Diego, *Progress in Energy and Combustion Science* **2012**, *38*, 215-282.

[9] J. C. Abanades, B. Arias, A. Lyngfelt, T. Mattisson, D. E. Wiley, H. Li, M. T. Ho, E. Mangano, S. Brandani, *Int. J. Greenh. Gas Con.* **2015**, *40*, 126-166.

[10] S. Noorman, M. van Sint Annaland, Kuipers, *Industrial & Engineering Chemistry Research* **2007**, *46*, 4212-4220.

[11] I. M. Dahl, E. Bakken, Y. Larring, A. I. Spjelkavik, S. F. Håkonsen, R. Blom, *Energy Procedia* **2009**, *1*, 1513-1519.

[12] H. P. Hamers, F. Gallucci, P. D. Cobden, E. Kimball, M. van Sint Annaland, *International Journal of Greenhouse Gas Control* **2013**, *16*, 1-12.

[13] M. Tang, L. Xu, M. Fan, *Applied Energy* **2015**, *151*, 143-156.

[14] A. Lyngfelt, T. Mattisson, *Vol.:Chapter 17, s. 475-504*, Efficient Carbon Capture for Coal Power Plants, Ed. Stolten, D., and Scherer, V., WILEY-VCH Verlag GmbH & Co.. KGaA, Weinheim, **2011**.

[15] Q. Imtiaz, D. Hosseini, C. R. Müller, *Energy Technology* **2013**, *1*, 633-647.

[16] A. Lyngfelt, *Applied Energy* **2014**, *113*, 1869-1873.

[17] A. Cuadrat, A. Abad, J. Adánez, L. F. de Diego, F. García-Labiano, P. Gayán, *Fuel Process. Technol.* **2012**, *94*, 101-112.

[18] M. Arjmand, H. Leion, T. Mattisson, A. Lyngfelt, *Applied Energy* **2014**, *113*, 1883-1894.

[19] H. Leion, E. Jerndal, B.-M. Steenari, S. Hermansson, M. Israelsson, E. Jansson, M. Johnsson, R. Thunberg, A. Vadenbo, T. Mattisson, A. Lyngfelt, *Fuel* **2009**, *88*, 1945-1954.

[20] A. Fossdal, E. Bakken, B. A. Øye, C. Schøning, I. Kaus, T. Mokkelbost, Y. Larring, *International Journal of Greenhouse Gas Control* **2011**, *5*, 483-488.

[21] J. Adánez, A. Cuadrat, A. Abad, P. Gayán, L. F. de Diego, F. García-Labiano, *Energy & Fuels* **2010**, *24*, 1402-1413.

[22] J. C. Abanades, B. Arias, A. Lyngfelt, T. Mattisson, D. E. Wiley, H. Li, M. T. Ho, E. Mangano, S. Brandani, *International Journal of Greenhouse Gas Control*.
[23] A. Cabello, A. Abad, P. Gayán, L. F. de Diego, F. García-Labiano, J. Adánez, *Energy Fuels* **2014**, *28*, 1262-1274.
[24] M. Pishahang, Y. Larring, M. McCann, R. Bredesen, *Ind. Eng. Chem. Res.* **2014**, *53*, 10549-10556.
[25] H. Leion, Y. Larring, E. Bakken, R. Bredesen, T. Mattisson, A. Lyngfelt, *Energy & Fuels* **2009**, *23*, 5276-5283.
[26] S. Sundqvist, H. Leion, M. Rydén, A. Lyngfelt, T. Mattisson, *Energy Technology* **2013**, *1*, 338-344.
[27] A. Abad, F. García-Labiano, P. Gayán, L. F. de Diego, J. Adánez, *Chemical Engineering Journal*.
[28] M. Pishahang, Y. Larring, M. F. Sunding, M. Jacobs, F. Snijkers, *Energy Technology* **2016**, *4*, 1305-1316.
[29] M. Rydén, A. Lyngfelt, T. Mattisson, *International Journal of Greenhouse Gas Control* **2011**, *5*, 356-366.
[30] P. Hallberg, D. Jing, M. Rydén, T. Mattisson, A. Lyngfelt, *Energy and Fuels* **2013**, *27*, 1473-1481.
[31] A. Fossdal, O. Darell, A. Lambert, E. Schols, E. Comte, R. Leenman, R. Blom, *Energy and Fuels* **2015**, *29*, 314-320.
[32] N. Galinsky, M. Sendi, L. Bowers, F. Li, *Applied Energy* **2016**, *174*, 80-87.
[33] P. Gayán, L. F. de Diego, F. García-Labiano, J. Adánez, A. Abad, C. Dueso, *Fuel* **2008**, *87*, 2641-2650.
[34] C. Linderholm, T. Mattisson, A. Lyngfelt, *Fuel* **2009**, *88*, 2083-2096.
[35] I. Adánez-Rubio, P. Gayán, A. Abad, L. F. de Diego, F. García-Labiano, J. Adánez, *Energy & Fuels* **2012**, *26*, 3069-3081.
[36] A. D. Salman, M. J. Hounslow, J. P. K. Seville, in *Handbook of Powder Technology, Vol. Volume 11* (Eds.: M. J. H. A.D. Salman, J. P. K. Seville), Elsevier Science B.V., **2007**.
[37] V. Thoréton, M. Pishahang, T. Mokkelbost, K. Wiik, Y. Larring, *Energy technology* **2017**.
[38] H. S. Horowitz, J. M. Longo, *Materials Research Bulletin* **1978**, *13*, 1359-1369.
[39] D. Jing, F. Snijkers, P. Hallberg, H. Leion, T. Mattisson, A. Lyngfelt, *Energy & Fuels* **2016**, *30*, 3257-3268.
[40] M. Källén, M. Rydén, C. Dueso, T. Mattisson, A. Lyngfelt, *Industrial & Engineering Chemistry Research* **2013**, *52*, 6923-6932.
[41] M. Rydén, P. Moldenhauer, S. Lindqvist, T. Mattisson, A. Lyngfelt, *Powder Technology* **2014**, *256*, 75-86.
[42] C. A. Schneider, W. S. Rasband, K. W. Eliceiri, *Nat Meth* **2012**, *9*, 671-675.
[43] T. Kanada, *Precision Engineering* **1997**, *20*, 117-122.
[44] J. Schindelin, I. Arganda-Carreras, E. Frise, V. Kaynig, M. Longair, T. Pietzsch, S. Preibisch, C. Rueden, S. Saalfeld, B. Schmid, J.-Y. Tinevez, D. J. White, V. Hartenstein, K. Eliceiri, P. Tomancak, A. Cardona, *Nat Meth* **2012**, *9*, 676-682.

374 Table 1. Life expectancy of OCM depending of the sintering conditions. $Ni/NiAl_2O_4$ was taken
375 as a reference.

Material	**Sintering in air**		**Life-time expectancy (hours)**
	Temperature (˚C)	Duration (hours)	
$Ni/NiAl_2O_4$ (VITO) [34]	–	–	33000
CMT	1280	12	6600
CMTF125	1200	6	–
CMTF125	1250	1	2700
CMTF125	1280	1/2	2700
CMTF125	1280	1	6600
CMTF125	1280	6	1100
CMTF125	1280	12	6600
CMTF125@Alumina	1280	1	6600

376

377 Table 2. Different samples and their compositions.

Material	**Cations stoichiometry**				**Sintering in air**	
	Ca	Mn	Ti	Fe	Temperature (˚C)	Duration (hours)
CMT	0.98	0.875	0.125	–	1280	6
CMT	0.98	0.875	0.125	–	1280	12
CMTF125	0.98	0.75	0.125	0.125	1200	6
CMTF125	0.98	0.75	0.125	0.125	1250	1
CMTF125	0.98	0.75	0.125	0.125	1280	1/2
CMTF125	0.98	0.75	0.125	0.125	1280	1
CMTF125	0.98	0.75	0.125	0.125	1280	6
CMTF125	0.98	0.75	0.125	0.125	1280	12
CMTF125@Alumina	0.98	0.75	0.125	0.125	1280	1
CMTF125@Alumina	0.98	0.75	0.125	0.125	1280	2
CMTF125@Alumina	0.98	0.75	0.125	0.125	1280	12

378

List of Figure Captions:

Figure 1. X-ray diffractograms of CMT (a), CMTF125 (b) and CMTF125@Alumina (c) granules after sintering at 1280˚C for different times.

Figure 2. SEM micrographs of sintered (1280 ˚C) and sieved granules of CMT (a) sintered for 12 hours and CMTF125 (b and c) respectively sintered for 1 and 12 hours. Details of the surface are shown in the inserts.

Figure 3. (a) Mean roundness of green-state granules as a function of particle size (hollow symbols) and corresponding particles size distribution (filled symbols) after sieving. (b) Volume density distributions of granules' roundness (sieved in the 125-180 μm range). Measurements were done before sintering.

Figure 4. SEM micrograph and corresponding EDS maps of the cross-section of a fresh CMT granule (a). Volume size distribution of the initial reactants (b).

Figure 5. SEM micrographs and corresponding EDS maps of Calcium, Manganese, Titanium and Iron of cross-sections of a CMT granule (a) sintered for 12 hours at 1280˚C in air, and CMTF125 granules (b and c), respectively sintered at 1200˚C for 6 hours and 1280˚C for 12 hour.

Figure 6. Specific surface area of CMTF125 granules as a function of sintering time at 1280˚C (main graph) and temperature (insert).

Figure 7. Fabricated colors combined EDS maps of cross sections of CMTF125@Alumina, sintered in air at 1280°C. Ti and Fe are on exactly on the same positions as Mn.

Figure 8. Mass loss over time during cold attrition test. Samples of CMTF125 were sintered at different temperatures and times.

400 Figure 9. Particle size of granules before (plain lines) and after (dashed lines) being exposed to
401 cold attrition test.

402 Figure 10. Principle of spray granulation and spray coating. Schematic from courtesy of Glatt.

403

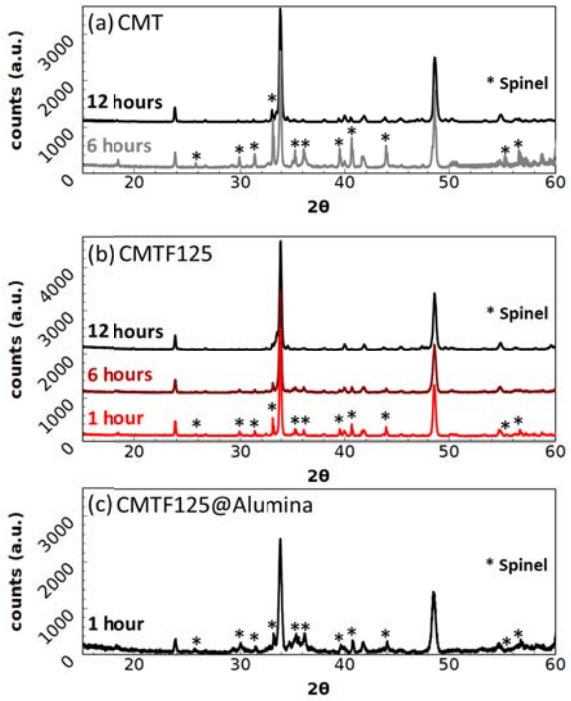

404

405 Figure 1. X-ray diffractograms of CMT (a), CMTF125 (b) and CMTF125@Alumina (c) granules

406 after sintering at 1280˚C for different times.

407

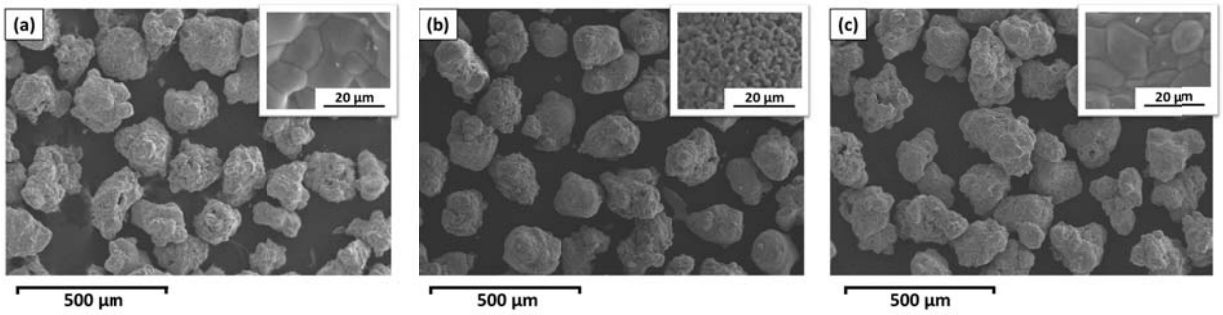

408

409 Figure 2. SEM micrographs of sintered (1280 ˚C) and sieved granules of CMT (a) sintered for 12

410 hours and CMTF125 (b and c) respectively sintered for 1 and 12 hours. Details of the surface are

411 shown in the inserts.

412

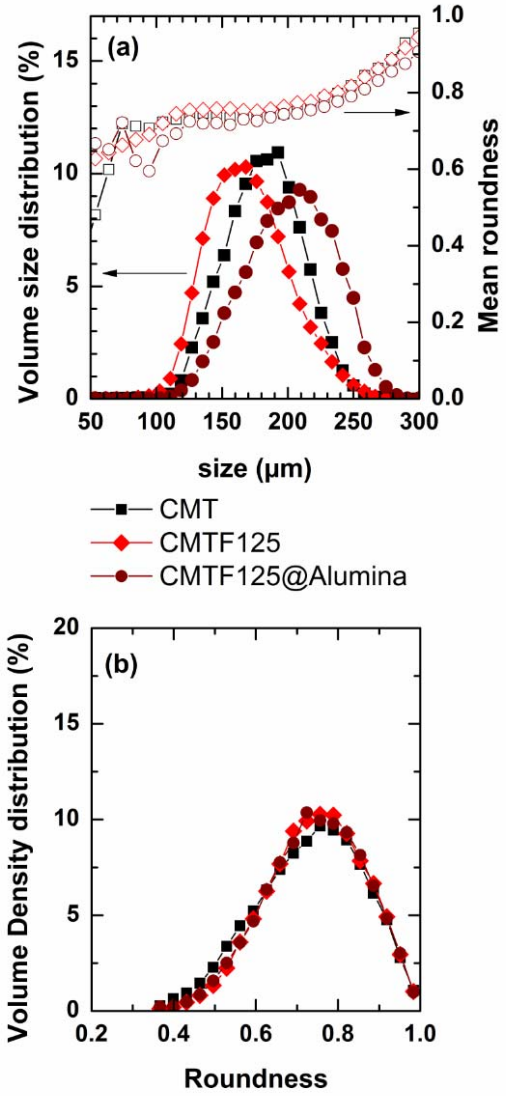

413

414 Figure 3. (a) Mean roundness of green-state granules as a function of particle size (hollow
415 symbols) and corresponding particles size distribution (filled symbols) after sieving. (b) Volume
416 density distributions of granules' roundness (sieved in the 125-180 μm range). Measurements
417 were done before sintering.

418 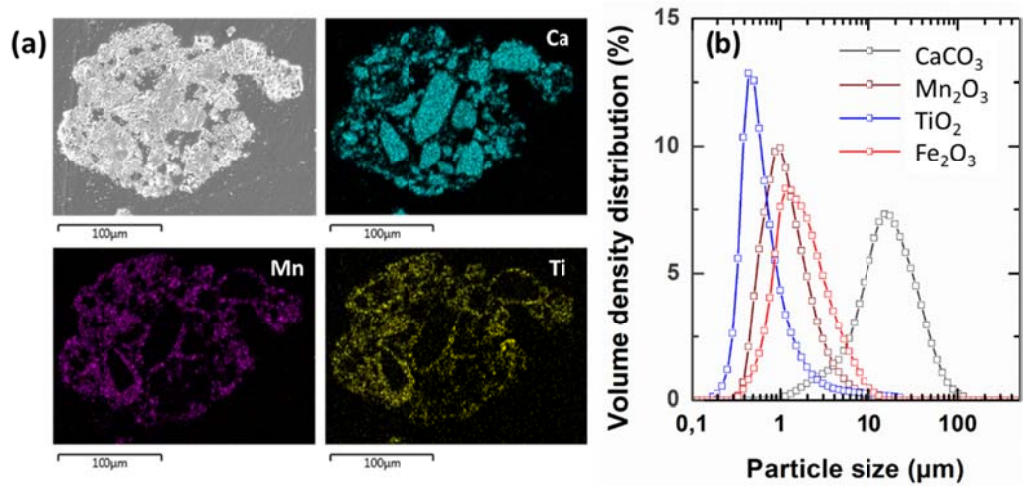

419 Figure 4. SEM micrograph and corresponding EDS maps of the cross-section of a fresh CMT
420 granule (a). Volume size distribution of the initial reactants (b).

421

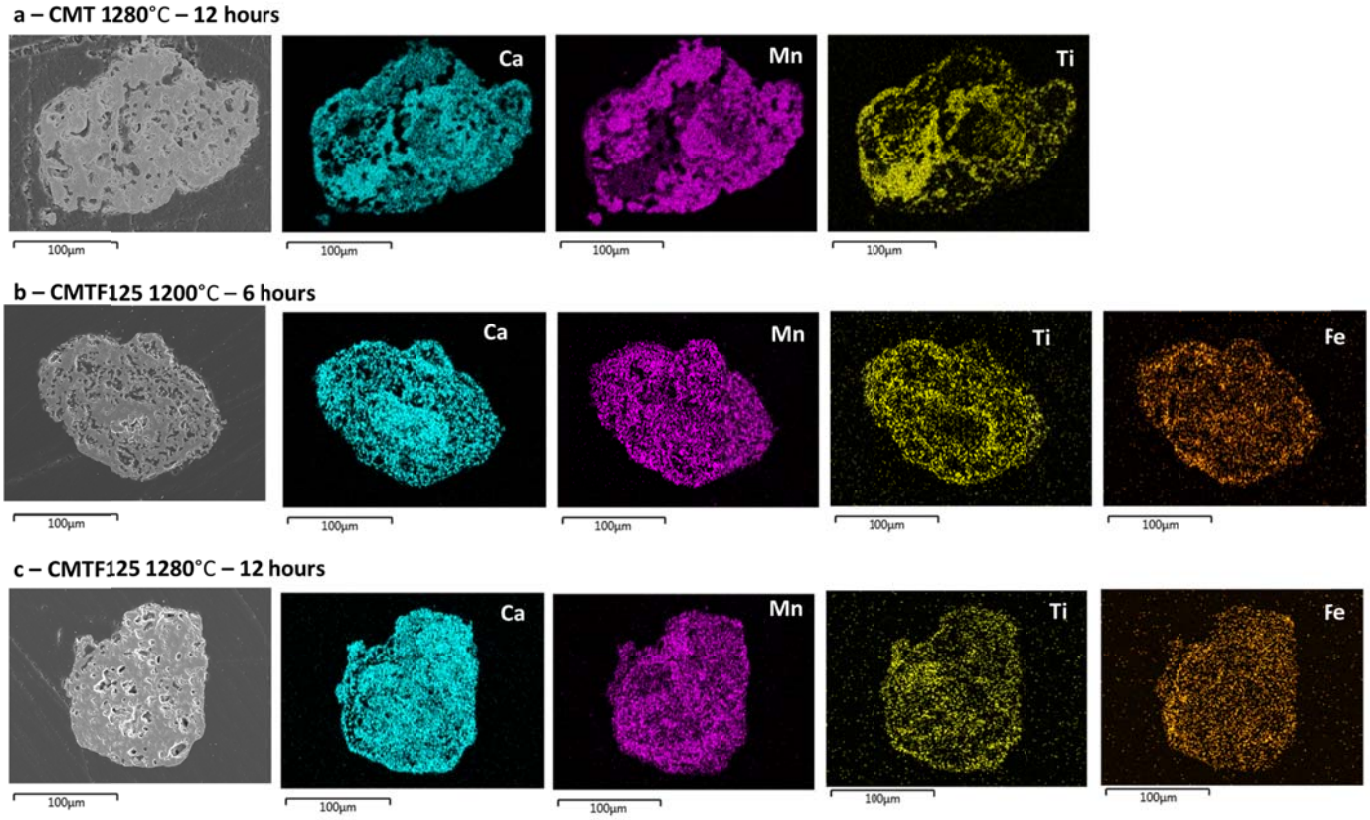

422

423 Figure 5. SEM micrographs and corresponding EDS maps of Calcium, Manganese, Titanium and

424 Iron of cross-sections of a CMT granule (a) sintered for 12 hours at 1280˚C in air, and CMTF125

425 granules (b and c), respectively sintered at 1200˚C for 6 hours and 1280˚C for 12 hour.

426

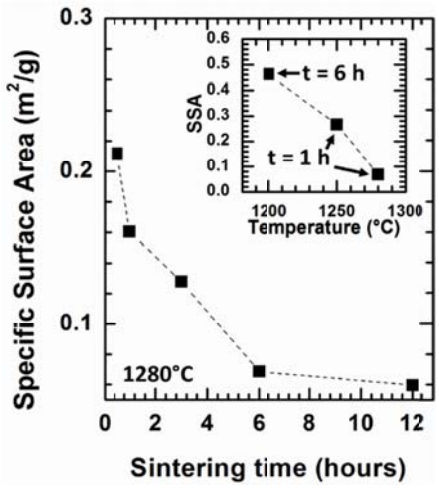

427

428 Figure 6. Specific surface area of CMTF125 granules as a function of sintering time at 1280˚C
429 (main graph) and temperature (insert).

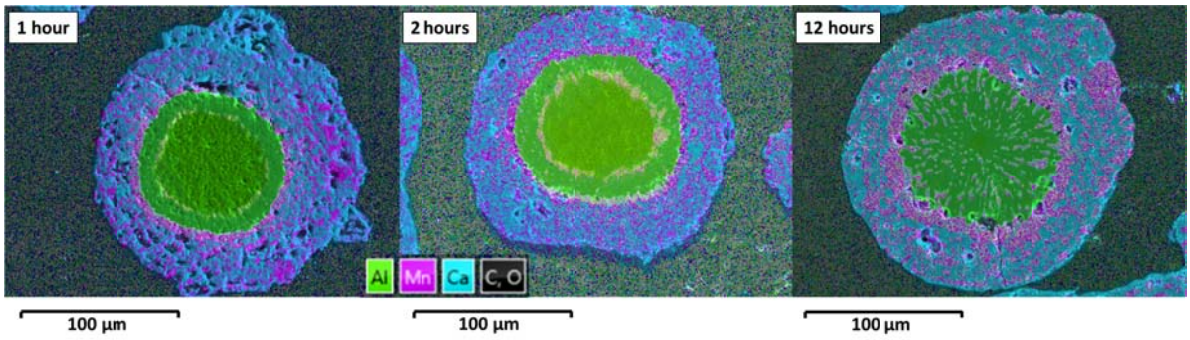

430

431 Figure 7. Fabricated colors combined EDS maps of cross sections of CMTF125@Alumina,
432 sintered in air at 1280°C. Ti and Fe are on exactly on the same positions as Mn.

433

434

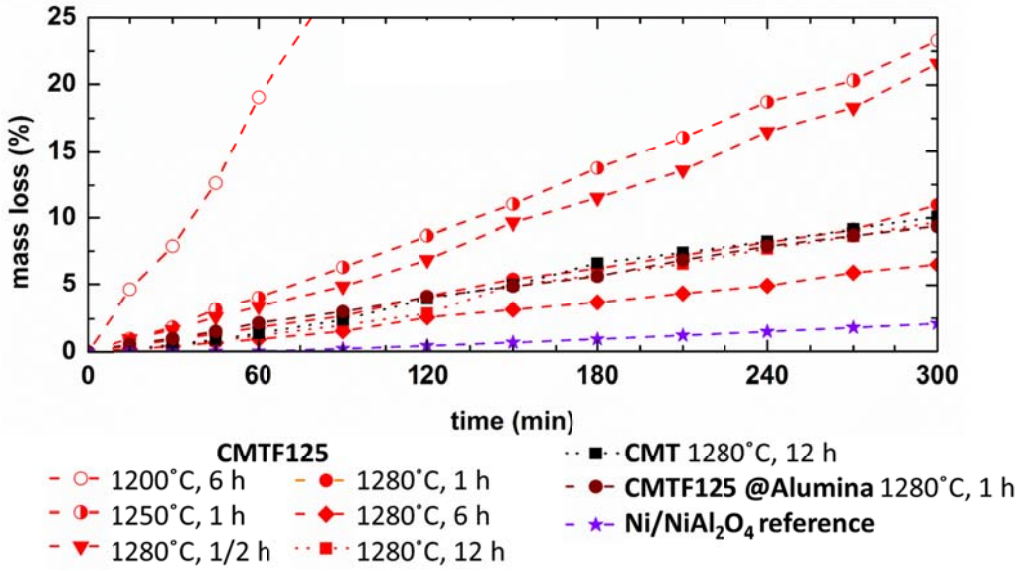

435

436 Figure 8. Mass loss over time during cold attrition test. Samples of CMTF125 were sintered at

437 different temperatures and times.

438

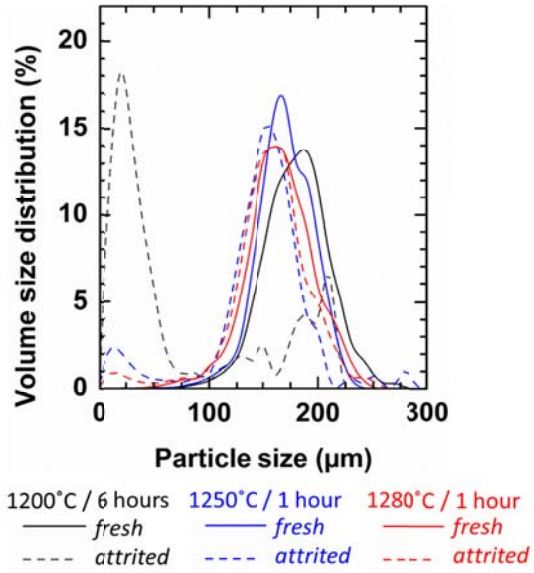

439

440 Figure 9. Particle size of granules before (plain lines) and after (dashed lines) being exposed to

441 cold attrition test.

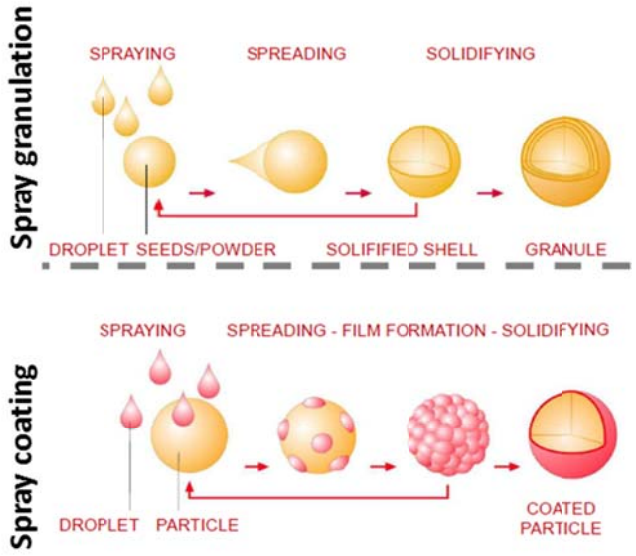

442

443 Figure 10. Principle of spray granulation and spray coating. Schematics courtesy of Glatt.

444

445

446 **Entry for the Table of Contents** (Please choose one layout)

447

FULL PAPER

*Vincent Thoréton, Ove Darell, Aud I Spjelkavik, Martin Fleissner Sunding, Tommy Mokkelbost, Mehdi Pishahang, Kjell Wiik, Yngve Larring**

Page No. – Page No.

Manufacturing of perovskite oxygen carriers by spray granulation for chemical looping combustion

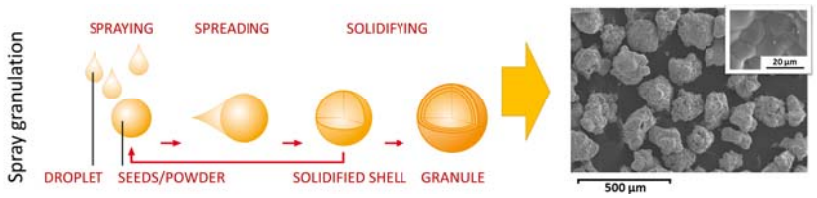

Spray granulation for making Oxygen Carriers for Chemical Looping Combustion: Here we demonstrate that spray granulation, a scalable industrial process, is relevant to manufacture promising Oxygen Carrier Materials for Chemical Looping Combustion from low cost and low environmental impact minerals and with good mechanical properties.

448